

SCIENTIFIC REPORTS



OPEN

Routes to Chaos Induced by a Discontinuous Resetting Process in a Hybrid Spiking Neuron Model

Sou Nobukawa¹, Haruhiko Nishimura² & Teruya Yamanishi³

Several hybrid spiking neuron models combining continuous spike generation mechanisms and discontinuous resetting processes following spiking have been proposed. The Izhikevich neuron model, for example, can reproduce many spiking patterns. This model clearly possesses various types of bifurcations and routes to chaos under the effect of a state-dependent jump in the resetting process. In this study, we focus further on the relation between chaotic behaviour and the state-dependent jump, approaching the subject by comparing spiking neuron model versions with and without the resetting process. We first adopt a continuous two-dimensional spiking neuron model in which the orbit in the spiking state does not exhibit divergent behaviour. We then insert the resetting process into the model. An evaluation using the Lyapunov exponent with a saltation matrix and a characteristic multiplier of the Poincaré map reveals that two types of chaotic behaviour (i.e. bursting chaotic spikes and near-period-two chaotic spikes) are induced by the resetting process. In addition, we confirm that this chaotic bursting state is generated from the periodic spiking state because of the slow- and fast-scale dynamics that arise when jumping to the hyperpolarization and depolarization regions, respectively.

Many types of neural coding (for e.g., rate, temporal, and population coding) are known to exist in brain/nerve system adaptive information processing¹. Many recent studies on the mechanisms of memory and learning in neural systems have utilised spiking neuron models that can recreate these types of neural coding by describing the spiking activity of the membrane potential^{1–5}.

The Hodgkin–Huxley neuron model⁶ is an important spiking neuron model that describes the dynamical evolution of the membrane potential and that of the gate variables associated with the K and Na ionic currents across the cellular membrane. This model comprises four equations involving several physiological parameters. Thus far, parameter values have been estimated for various types of neurons ranging from enormous squid axons to cortex neurons^{6–9}. However, the systems that are obtained when the Hodgkin–Huxley neuron model is used to construct large-scale neural systems include many variables and parameters, approaching the scale of an actual brain neural network. Therefore, applicable analytical approaches are limited and the computational load of the numerical calculation becomes high.

Simplified models described by continuous differential equations have been proposed to overcome this difficulty. These models retain the minimum required bifurcations and spiking patterns (e.g. the FitzHugh–Nagumo neuron model^{10,11} and the Hindmarsh–Rose neuron model¹²).

Meanwhile, several hybrid spiking neuron models combining continuous spike generation mechanisms and discontinuous resetting processes after spiking have been proposed as simple transition schemes for membrane potentials between spiking and part of the hyperpolarization^{13–16}. For example, the Izhikevich neuron model can reproduce nearly all spiking activities observed in actual neural systems by tuning a few parameters, including those relating to the resetting process^{13,14}. Furthermore, in their use of non-linear integrate-and-fire models as hybrid spiking neuron models, Badel *et al.*¹⁷ proposed a possible method for estimating optimal parameter values using data obtained from a single neuron via intracellular voltage recording. They reported an extremely high fitting accuracy in reproducing spike patterns and were able to rapidly estimate parameters.

The hybrid spiking neuron model is a piecewise-smooth system in which the dynamics are switched according to the system's state¹⁸. Saito *et al.* conducted chaos and bifurcation analysis and circuit implementation using

¹Department of Computer Science, Chiba Institute of Technology, 2-17-1 Tsudanuma, Narashino, Chiba, 275-0016, Japan. ²Graduate School of Applied Informatics, University of Hyogo, 7-1-28 Chuo-ku, Kobe, Hyogo, 650-8588, Japan.

³Department of Management Information Science, Fukui University of Technology, 3-6-1 Gakuen, Fukui, 910-8505, Japan. Correspondence and requests for materials should be addressed to S.N. (email: nobukawa@cs.it-chiba.ac.jp)

the piecewise-constant and piecewise-linear systems as types of piecewise-smooth systems^{19–23}. Tsubone *et al.*²³ proposed a systematic method using an analytical approach to predict the parameter regions for the chaotic states in piecewise-constant systems. Meanwhile, Mitsubori and Saito¹⁹ and Nakano and Saito²⁰ developed a systematic method for piecewise-linear systems. However, the analysis of chaos and bifurcation in piecewise-smooth systems such as the Izhikevich neuron model, which generally include non-linear terms, requires the evaluation of the Lyapunov exponents and characteristic multipliers against exhaustive parameter sets. Several indices considering the effect of the resetting process using the saltation matrix have been proposed^{16,24–27}. Coombes *et al.*¹⁶ utilised this approach and conducts an analysis of the planar non-linear integrate-and-fire model in a large parameter region. They revealed that the parameter region for chaotic states is located at the boundary between burst firing and fast spiking. The Izhikevich neuron model clearly features various types of bifurcation and routes to chaos under the effect of the state-dependent jump in the resetting process^{27–31}. However, neither the relation between the chaotic behaviours and the state-dependent jump nor the mechanism for inducing the chaotic states using the resetting process has been revealed.

Revealing this mechanism requires evaluating the influence of the state-dependent jump on the trajectory in a continuous system through a comparison of two systems: versions with and without the resetting process. The aforementioned Izhikevich neuron model cannot be applied for this purpose because of its divergent behaviour in the spiking state when the resetting process is removed. We previously introduced a preliminary approach to this issue based on a comparison of spiking neuron models such as the FitzHugh–Nagumo neuron model with and without the resetting process^{32,33}. In actual neural systems, the system state transits from resting to spiking through both Hopf and saddle-node bifurcations^{1,34}. However, the FitzHugh–Nagumo neuron model permits spiking activity only via Hopf bifurcation. A non-linear equation for the membrane recovery variable with a sigmoidal function has been reported to generate spiking activity via both types of bifurcation³⁴.

In our approach, we first adopt a continuous two-dimensional (2D) spiking neuron model with a non-linear equation for the recovery variable in which the orbit in the spiking state does not exhibit divergent behaviour. We then add the resetting process to the model. Utilising a rigorous method to analyse the bifurcation and chaos in hybrid systems (i.e., using a characteristic multiplier of the Poincaré map and Lyapunov exponents with a saltation matrix), we evaluate several routes to chaos, which cannot be achieved in a hybridised FitzHugh–Nagumo neuron model³³, by changing the resetting process parameters and comparing the structure of the attractor between the system versions with and without the resetting process.

Model and Method

Spiking Neuron Model with the Resetting Process. The FitzHugh–Nagumo neuron model^{10,11} is driven by 2D ordinary differential equations with the following form:

$$\dot{v} = v(a - v)(v - 1) - u + I, \quad (1)$$

$$\dot{u} = bv - cu, \quad (2)$$

where v and u represent the membrane potential of a neuron and the membrane recovery variable, respectively. The parameter a determines the shape of a v -nullcline ($\dot{v} = 0$), while b/c and c exhibit the sensitivity of u and its time constant, respectively. In real-world neural systems, the system state transits from resting to spiking through both Hopf and saddle-node bifurcations^{1,34}. However, the FitzHugh–Nagumo model only permits spiking activity via Hopf bifurcation. Spiking neuron models such as the Morris–Lecar neuron model³⁵ can be used to generate spiking activity via both types of bifurcation. Such models apply the following non-linear equation for \dot{u} with a sigmoidal function for v ^{34,36}:

$$\dot{u} = \alpha \left(\frac{1}{1 + \exp(-(v - \beta)/\varepsilon)} - u \right), \quad (3)$$

where α is the time constant for u and parameters β and ε determine the shape of the sigmoidal function. Instead of the linear equation given by Eq. (2), we use Eq. (3) with the parameters set to $(a, \alpha, \varepsilon) = (0.1, 0.1, 0.05)$ as the equation for \dot{u} .

For the continuous spiking neuron model above, we implement the resetting process given by the following equation:

$$\text{if } v \geq v_{\text{peak}}, \text{ then } \begin{cases} v \rightarrow v_r, \\ u \rightarrow u + d, \end{cases} \quad (4)$$

where v_r and d represent the after-spike reset values of the membrane potential v and the recovery variable u , respectively. In other words, we consider it to be a spike event if v reaches v_{peak} . The state-dependent jump induced by Eq. (4) converges to a continuous trajectory under the condition $v_r \rightarrow v_{\text{peak}}$ and $d \rightarrow 0$ in the case which v_{peak} is set to a maximum value of v for the orbit of the continuous spiking neuron model given by Eqs (1) and (3).

We numerically analysed this model in SUNDIALS, our non-linear differential/algebraic equation solver simulator, using the backward-differentiation formula method with Newton's iteration³⁷. As this function can detect intersection points between a trajectory and the user-defined manifolds, we utilise it to detect the points for $v \geq v_{\text{peak}}$. The time step for numerical integration is related to the time precision needed to detect intersection points. As the fixed width in this solver is not user-tunable, relative and absolute tolerances are set instead; we set these to sufficiently small values (10^{-14}) to achieve sufficient numerical precision for the evaluation of a chaotic spiking activity and the detection of the intersection.

Evaluation Indices. *Lyapunov exponents.* Lyapunov exponents with saltation matrices are utilised here to quantify the chaotic activity in the version of the spiking neuron model with the resetting process^{25,26,28}. The evolution of the orthogonal vectors of perturbation \mathbf{I}_j ($j = 1, 2$) for Eqs (1) and (3) in a system with a continuous trajectory in spike intervals between the i -th and $(i + 1)$ -th times ($t_i \leq t \leq t_{i+1}$) is described as follows:

$$\dot{\Lambda}^{i+1}(t, t_i) = J(v, u, t)\Lambda^{i+1}(t, t_i), \tag{5}$$

where Λ^{i+1} is the matrix $(\mathbf{I}_1, \mathbf{I}_2)$. The Jacobian matrix J for Eqs (1) and (3) is given as follows:

$$J = \begin{bmatrix} -3v^2 + 2(a + 1)v - a & -1 \\ \alpha \frac{1}{\varepsilon 1 + \exp((-v - \beta)/\varepsilon)} \left(1 - \frac{1}{1 + \exp((-v - \beta)/\varepsilon)} \right) & -\alpha \end{bmatrix}. \tag{6}$$

\mathbf{I}_j is corrected by Gram–Schmidt orthonormalisation at intervals of 10^{-3} to maintain the orthogonality of \mathbf{I}_j :

$$\mathbf{I}_1^\perp \rightarrow \mathbf{I}_1, \tag{7}$$

$$\mathbf{I}_2^\perp \rightarrow \mathbf{I}_2 - \frac{\mathbf{I}_1 \cdot \mathbf{I}_2}{|\mathbf{I}_1|} \mathbf{I}_1^\perp, \tag{8}$$

$$\Lambda^{i+1} \rightarrow (\mathbf{I}_1^\perp, \mathbf{I}_2^\perp). \tag{9}$$

The saltation matrix at $t = t_i$ is given by the following equation:

$$S_i = \begin{bmatrix} \frac{v^+}{v^-} & 0 \\ \frac{u^+ - u^-}{v^-} & 1 \end{bmatrix}, \tag{10}$$

where (v^-, u^-) and (v^+, u^+) represent the values of (v, u) before and after spiking, respectively. $\Lambda^k(T^{k+1}, T^k)$ ($k = 0, 1, \dots, N-1$) can be expressed as follows in case spikes arise in the range $[T^k, T^{k+1}]$ ²⁸:

$$\Lambda^k(T^{k+1}, T^k) = \Lambda_{i+1}(T^{k+1}, t_i) S_i \Lambda_i(t_i, t_{i-1}) \dots S_2 \Lambda_2(t_2, t_1) S_1 \Lambda_1(t_1, T^k), \tag{11}$$

$$\Lambda^k(T^k, T^k) = (\mathbf{I}_1/|\mathbf{I}_1|, \mathbf{I}_2/|\mathbf{I}_2|). \tag{12}$$

The initial perturbation $\Lambda^0(T^0, T^0)$ and the evolution period $\tau = T^{k+1} - T^k$ are set to unit matrix E and 0.1, respectively.

The Lyapunov spectrum λ_j is calculated as follows based on the norm of \mathbf{I}_j^k ($j = 1, 2$) in $\Lambda^k(T^{k+1}, T^k)$:

$$\lambda_j = \frac{1}{N\tau} \sum_{k=0}^{N-1} \log(|\mathbf{I}_j^k|), \tag{13}$$

where the evolution period for λ_j is set to $N\tau = 10^5$ ($N = 10^8, \tau = 10^{-3}$).

Poincaré map. We set a Poincaré section $\Psi(v = v_{\text{peak}})$ to conduct a bifurcation analysis in a system with a state-dependent jump. The dynamics of the system behaviour on Ψ are given by the Poincaré map as follows:

$$u_{i+l} = \psi^l(u_i) \quad (l = 1, 2, \dots). \tag{14}$$

We evaluate here the profile of ψ^l on a return map of $u_i - u_{i+l}$. In practice, we solve Eqs (1),(3) and (4) against the initial values of (v_r, u_0) , and obtain the u values that pass through Ψ at times l as u^l . The values (u_0, u_l) are plotted on a return map of $u_i - u_{i+l}$.

Characteristic multiplier of the Poincaré map. The variational equations of Eqs (1) and (3) in a system with a continuous trajectory in spike intervals between the i -th and $(i + 1)$ -th times ($t_i \leq t \leq t_{i+1}$) are defined as follows:

$$\dot{\Phi}_{i+1}(t, t_i) = J(v, u, t)\Phi_{i+1}(t, t_i), \tag{15}$$

where Φ indicates the state transition matrix. $\Phi(t, t_0)$ can be expressed as follows for the case in which spikes arise in the range $[t : t_0]$:

$$\Phi(t, t_0) = \Phi_{i+1}(t, t_i) S_i \Phi_i(t_i, t_{i-1}) \dots S_2 \Phi_2(t_2, t_1) S_1 \Phi_1(t_1, 0). \tag{16}$$

The initial state transition $\Phi(t_0, t_0)$ is set here as the unit matrix E .

We calculate the characteristic multiplier of the solution for the l period ($u_0 = \psi^l(u_0)$) as follows:

$$\mu^l = \frac{\partial \psi^l}{\partial u_0}, \quad (17)$$

where u_0 indicates the initial value of orbit $\mathbf{x}_0 = (v_r, u_0)$ at $t = t_0$. The projection P and embedding P^{-1} to and from the Poincaré section are defined as follows by local sections Π_0 and Π_1 , respectively:

$$P : \Pi_0 \rightarrow \Psi \quad \mathbf{x} \rightarrow w = u, \quad (18)$$

$$P^{-1} : \Psi \rightarrow \Pi_0 \quad u \rightarrow \mathbf{x} = \begin{pmatrix} v_r \\ u \end{pmatrix}, \quad (19)$$

where w indicates the local coordinate on Ψ . According to the literature²⁷, local sections Π_0 and Π_1 are set as follows to solve Eq. (17):

$$\Pi_0 = \{\mathbf{x} = (v, u) \in \mathbb{R}^2 | q_0(v, u) = v - v_r = 0\}, \quad (20)$$

$$\Pi_1 = \{\mathbf{x} = (v, u) \in \mathbb{R}^2 | q_1(v, u) = v - c = 0\}, \quad (21)$$

where $q_0(v, u)$ and $q_1(v, u)$ are the scalar functions used to determine the local sections. Eq. (17) can be developed as follows to utilise the aforementioned sets (see the detailed derivation from Eq. (22) to Eq. (23) in ref.²⁷):

$$\mu^l = \frac{\partial \psi^l}{\partial \mathbf{u}_0} = \frac{\partial P}{\partial \mathbf{x}} \frac{\partial \psi^l}{\partial \mathbf{x}_0} \frac{\partial P^{-1}}{\partial w} \quad (22)$$

$$= (0 \ 1) \begin{pmatrix} 0 & 0 \\ -\dot{v}/\dot{u} & 1 \end{pmatrix} \Phi(t_r, t_0) \begin{pmatrix} 0 \\ 1 \end{pmatrix}. \quad (23)$$

$|\mu^l| < 1$, $\mu^l = -1$ and $\mu^l = 1$ represent the stable condition, period-doubling bifurcation and tangent bifurcation, respectively.

Results

Bifurcation in a Continuous 2D Spiking Neuron Model.

First, we demonstrate the system behaviour of the continuous spiking neuron model given by Eqs (1) and (3) for the cases of $\beta = 0.5$ and $\beta = 0.3$, which are hereinafter called regions #1 and #2, respectively. For region #1, Fig. 1(a) shows the v -nullcline ($\dot{v} = 0$), u -nullcline ($\dot{u} = 0$) and vector field of (\dot{v}, \dot{u}) in the case $I = 0$; these are denoted by a dotted line, a dashed line, and arrows, respectively. In this region, the fixed points (i.e. the points at which the v -nullcline intersects with the u -nullcline) are located at $(v, u) \approx (0, 0)$, $(0.10, 0)$, $(0.35, 0.06)$. The system trajectories are attracted to the stable fixed point $((v, u) \approx (0, 0))$. The other intersection points are unstable fixed points. In the $I = 0.004$ case (upper panel of Fig. 1(c)), the orbit indicated by a solid line exhibits a limit cycle along the vector field because of the effects of the destruction of the pair of stable and unstable fixed points. Next, as shown in the lower panel of Fig. 1(c), a spiking activity appears in the time series of $v(t)$. In region #2, the fixed point is located at $(v, u) \approx (0, 0)$, and, as the point is stable, the system trajectories are attracted to it (Fig. 1(b)). Meanwhile, in the $I = 0.04$ case, a limit cycle emerges as a result of the destabilisation of the fixed point (Fig. 1(d)).

We evaluate the eigenvalues m_j ($j = 1, 2$) of J around the stable fixed point $((v, u) \approx (0, 0))$ to specify the bifurcation against I . Figure 2(a) shows the dependence of the maximum real part of eigenvalue $\max_j \text{Re}(m_j)$ on I . The fixed point is stable ($\max_j \text{Re}(m_j) < 0$) in $-0.005 \leq I \lesssim 0.0024$, but disappears when $I \gtrsim 0.0024$. Furthermore, the limit cycle can be interpreted to be generated through saddle-node bifurcation because the complex values of m_j , m_1 and m_2 are real numbers in $0.0009 \lesssim I \lesssim 0.0024$ and m_2 reaches $\text{Re}(l_2) = 0$ at $I \approx 0.0024$, as shown in the left panel of Fig. 2(b). For region #2, the right panel of Fig. 2(a) shows the dependence of $\max_j \text{Re}(m_j)$ on I . In this region, the fixed point is stable in $-0.005 \leq I \lesssim 0.0193$ but becomes unstable when $I \gtrsim 0.0193$ because the complex values of m_j , m_1 and m_2 are complex conjugates and pass through a real axis at $I \approx 0.0193$ (right panel of Fig. 2(b)). Therefore, this bifurcation is classified as Hopf bifurcation.

Bifurcation and Chaos in the Spiking Neuron Model with the Resetting Process.

We evaluate the system's behaviour in the version of the spiking neuron model with the resetting process given by Eqs (1), (3) and (4). Figure 3 shows the dependence of the maximum Lyapunov exponent of λ_1 on parameters v_r and d in regions #1 (a) and #2 (b), respectively. The parameters for Eqs. (1) and (3) are set to $a = 0.1$, $\alpha = 0.1$, $\varepsilon = 0.05$; $\beta = 0.5$, $I = 0.004$ (region #1), $\beta = 0.3$, $I = 0.04$ (region #2) in the same manner as in the cases shown in Fig. 1(c) and (d). Parameter v_{peak} in Eq. (4) is set to 0.4 and 0.225 in regions #1 and #2, respectively. The chaotic state is induced by the resetting process in $0.25 \lesssim v_r \lesssim 0.4$, $0 \lesssim d \lesssim 0.025$ (region #1) and $0.12 \lesssim v_r \lesssim 0.17$, $0 \lesssim d \lesssim 0.01$ (region #2).

Figure 4 shows the dependence of the bifurcation diagrams of u_i and λ_j ($j = 1, 2$) on the v_r parameter in regions #1 and #2 with the value of parameter d fixed at $d = 0.01$ in Fig. 3. This result shows the chaotic states, which exhibit an irregular behaviour of u_i , and the Lyapunov exponents $\lambda_1 > 0$, $\lambda_2 = 0$ in region #1 observed in the parameter set for $(0.322 \lesssim v_r \lesssim 0.388)$. We evaluate the bifurcation against the chaotic region. The period-doubling and tangent bifurcations arise at $v_r \approx 0.288$ ($l = 1$), 0.318 ($l = 2$), 0.322 ($l = 4$), ... and $v_r \approx 0.388$ ($l = 5$). Therefore, the aforementioned chaotic region is produced by period-doubling bifurcation in the positive

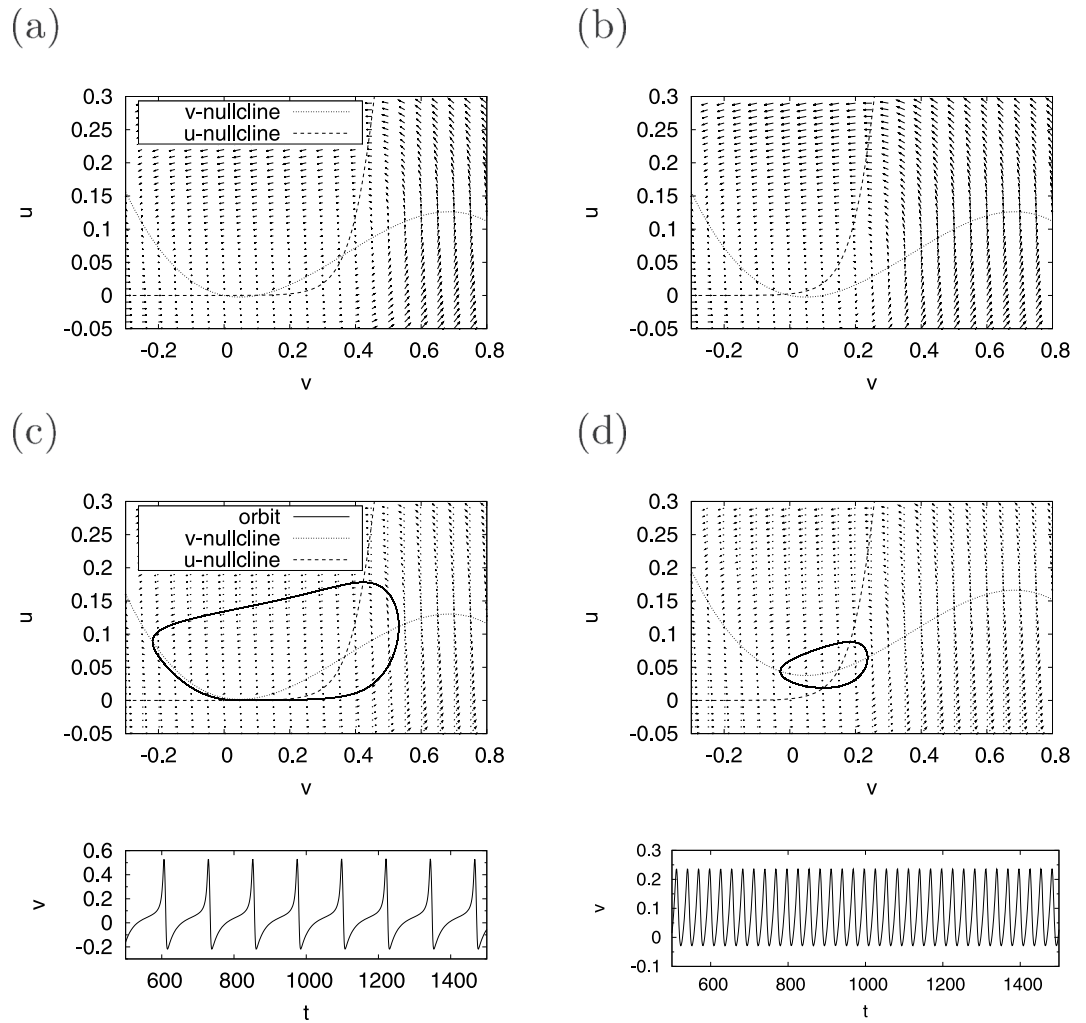


Figure 1. System behaviour in the continuous spiking neuron model. Orbit of (v, u) under the condition of no application of a direct current $I=0$ in regions #1 (a) and #2 (b); the orbit of (v, u) (upper) and the time series of v (lower) under the condition with application of a direct current in regions #1 ($I=0.004$) (c) and #2 ($I=0.04$) (d). ($a=0.1, \alpha=0.1, \varepsilon=0.05; \beta=0.5$ (region #1), $\beta=0.3$ (region #2)).

direction of v_r , and by tangent bifurcation in the negative direction. The chaotic state ($\lambda_1 > 0, \lambda_2 = 0$) in region #2 is observed in $0.136 \lesssim v_r \lesssim 0.141$ (Fig. 4(b)). Tangent bifurcation arises at both sides of this chaotic region ($v_r \approx 0.136$ ($l=2$), 0.141 ($l=1$)). In other words, this chaotic region is induced by tangent bifurcation.

The upper panel of Fig. 5(a) shows the time series of $v(t)$ as an example of the chaotic spiking pattern in region #1 ($v_r=0.33, d=0.01$). In this spiking pattern, $v(t)$ exhibits two types of behaviours after the resetting process (spike). In one case, $v(t)$ enters the hyperpolarization mode and decreases to $v(t) \approx 0.25$. In the other case, $v(t)$ increases to v_{peak} but does not do so through hyperpolarization. This spike repeats several times. In the former behaviour, (v, u) jumps in the region of $\dot{v} < 0$ through the v -nullcline in the v - u phase plane, as shown in the lower panel in Fig. 5(a). Meanwhile, in the latter behaviour, (v, u) jumps in the region of $\dot{v} > 0$ but not do so through the v -nullcline via the resetting process. This spiking pattern is called a burst and is observed in actual neural systems. Figure 6 shows the bifurcation diagram after the value of $u_i + d$ is reset (a) and typical orbits at $v_r=0.25, 0.3, 0.32$ (b) for the transition scheme from spike to burst against changing v_r . This result implies that (v, u) jumps in the region of $\dot{v} < 0$ at $v_r \approx 0.31$ (see typical examples $v_r=0.25, 0.3$ in Fig. 6(b)). Meanwhile, at $v_r \gtrsim 0.31$, (v, u) jumps in the region of $\dot{v} > 0$ as well as in the region of $\dot{v} < 0$ (red circle in the $v_r=0.32$ graph in Fig. 6(b)). The upper and lower panels of Fig. 5(b) show examples of the chaotic time series of $v(t)$ and the behaviour of (v, u) in the v - u phase plane in region #2 ($v_r=0.14, d=0.01$). In this case, (v, u) always jumps in the region $\dot{v} > 0$ and the orbit exhibits a near-period-2 chaotic behaviour. We can also confirm the aforementioned mechanisms for generating a chaotic bursting behaviour and a near-period-2 chaotic behaviour in the Izhikevich neuron model^{29,31}.

Next, we investigate the dependence of the return map on v_r . For region #1, Fig. 7(a) shows $\psi(u_i)$ on the $u_{i+1} - u_i$ return map in cases with the resetting process, in which $v_r=0.15, v_r=0.33$ (corresponding to the value of v_r in Fig. 5(a)) and $v_r=0.395$, and in the case without the resetting process. In the case without the resetting process, which is indicated by the dotted black line, $\psi(u_i)$ exhibits a nearly constant value (≈ 0.01). Meanwhile, in

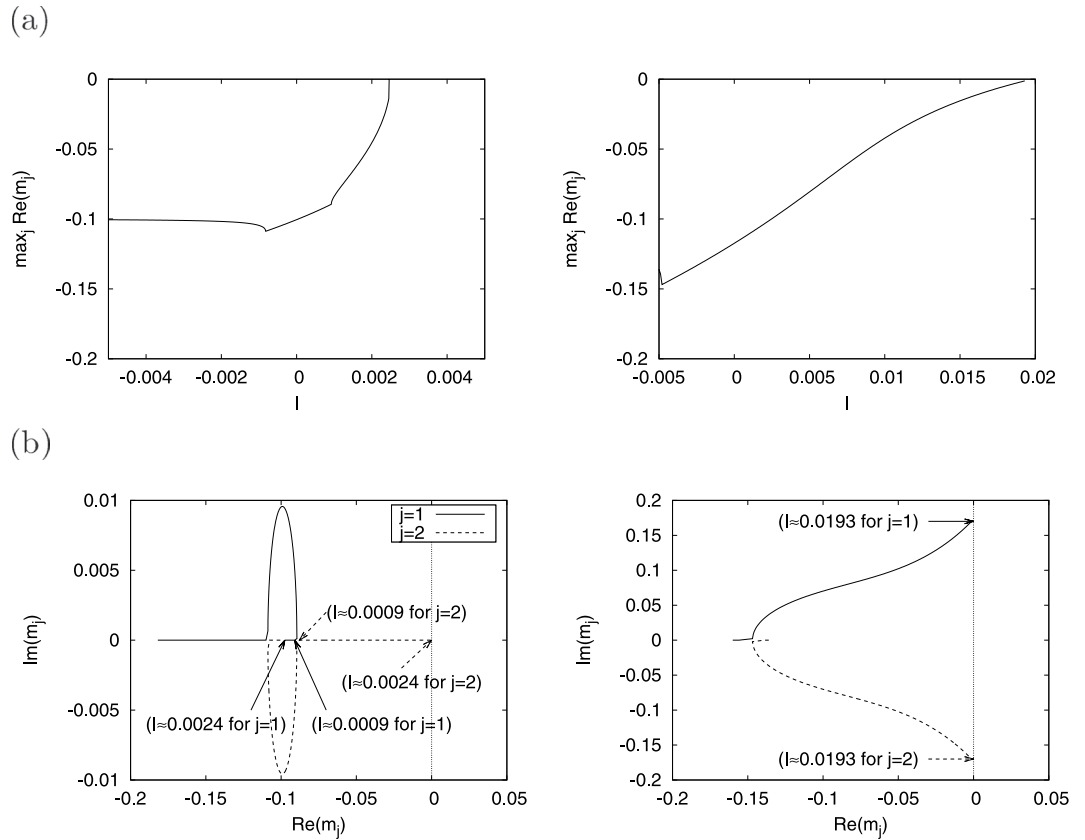


Figure 2. Dependence of the maximum real part of eigenvalue m_j ($j=1, 2$) on parameter I (a) and dependence of m_j on parameter I (b) in regions #1 (left) and #2 (right). ($a=0.1, \alpha=0.1, \varepsilon=0.05; \beta=0.5$ (region #1), $\beta=0.3$ (region #2)).

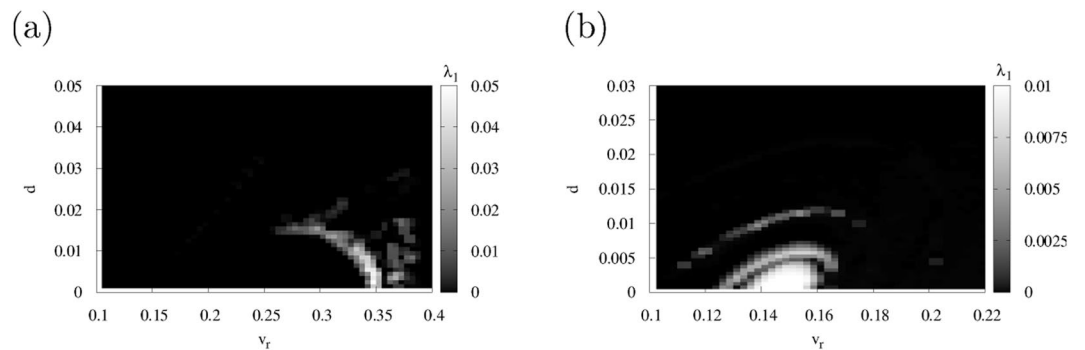


Figure 3. Maximum Lyapunov exponent λ_1 as a function of v_r and d around the chaotic region ($a=0.1, \alpha=0.1, \varepsilon=0.05$). (a) Region #1 ($\beta=0.5, I=0.004, v_{\text{peak}}=0.4$). (b) Region #2 ($\beta=0.3, I=0.04, v_{\text{peak}}=0.225$).

the cases in which the resetting process is applied the stretching and folding structure with piecewise nearly linear maps ($\psi(u_i) \approx u_i + 0.01$ if $-0.02 \lesssim u_i \lesssim 0.06$ and $\psi(u_i) \approx 0.01$ if $0.06 \lesssim u_i \lesssim 0.1$) in the $v_r=0.395$ case is indicated by the solid blue line. In the case of $v_r=0.33$, in which the distance of the jump in the $v-u$ phase plane becomes larger than $v_r=0.395$ as a result of separation from $v_{\text{peak}}=0.4$, a stretching and folding structure with non-linearity emerges at $u_i \approx 0.04$. The chaotic spiking activity observed in Fig. 5(a) can be considered to be induced by this structure. The stretching and folding structure then fades as v_r further decreases, as in the $v_r=0.15$ case indicated by the solid red line. For region #2, Fig. 7(b) shows $\psi(u_i)$ on the $u_{i+1}-u_i$ return map in the cases with the resetting process, in which $v_r=0.12, v_r=0.14$ (corresponding to the value of v_r in Fig. 5(b)), and $v_r=0.20$, and in the case without the resetting process. $\psi(u_i)$ is a nearly constant value in the case without the resetting process (≈ 0.03), which is indicated by the dotted black line, as well as for region #1. However, the stretching and folding structure arises as an effect of the resetting process ($v_r=0.20$ case, indicated by the solid blue line). Meanwhile, the frequency of the stretching and folding structure increases in the case in which the jump distance

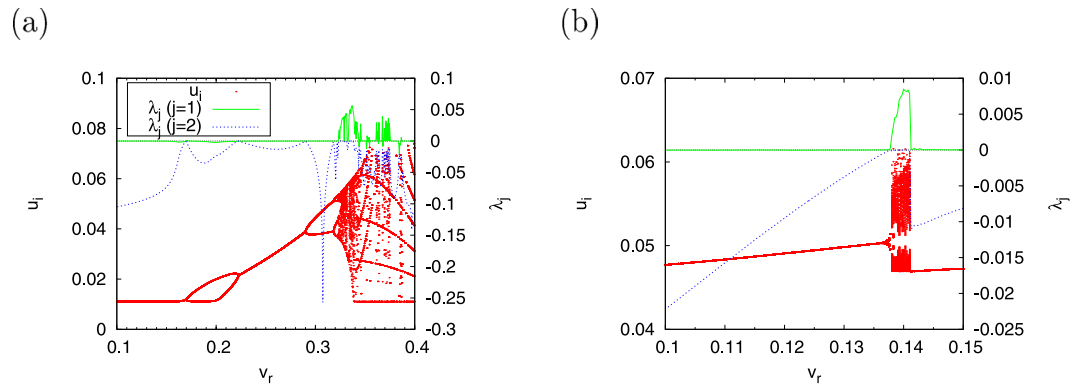


Figure 4. Bifurcation diagram and Lyapunov exponents λ_j ($j=1, 2$) as functions of v_r around the chaotic region ($a=0.1$, $\alpha=0.1$, $\varepsilon=0.05$). (a) Region #1 ($\beta=0.5$, $I=0.004$, $v_{\text{peak}}=0.4$, $d=0.01$). (b) Region #2 ($\beta=0.3$, $I=0.04$, $v_{\text{peak}}=0.225$, $d=0.01$).

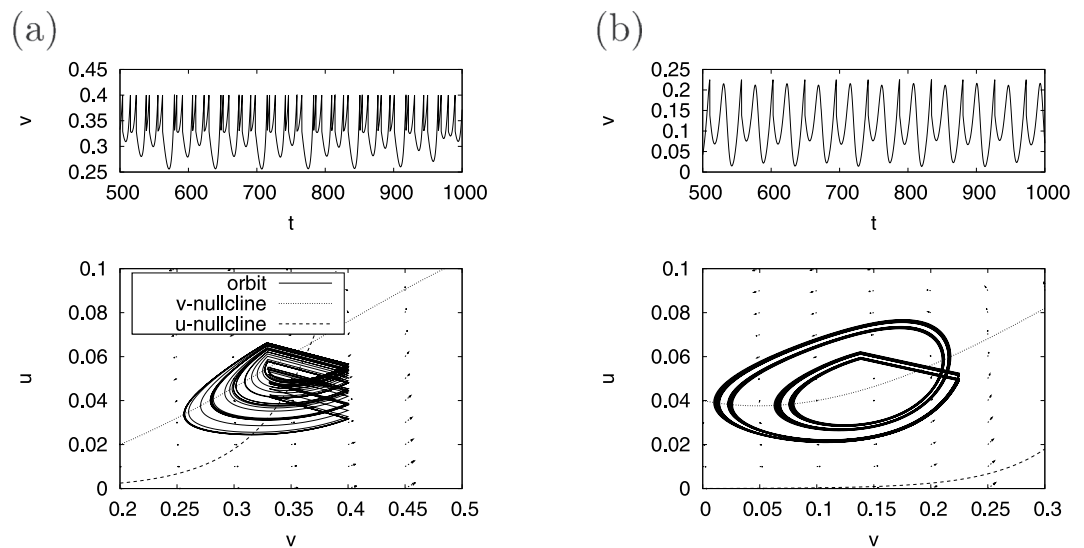


Figure 5. Chaotic time series of $v(t)$ (upper) and the orbit of (v, u) (lower) in the spiking neuron model with a state-dependent jump in regions #1 (a) and #2 (b). ($a=0.1$, $\alpha=0.1$, $\varepsilon=0.05$. Region #1: $\beta=0.5$, $I=0.004$, $v_{\text{peak}}=0.4$, $v_r=0.33$ and $d=0.01$; and region #2: $\beta=0.3$, $I=0.04$, $v_{\text{peak}}=0.225$, $v_r=0.14$ and $d=0.01$).

is larger than $v_r=0.20$ ($v_r=0.14$ case indicated by the solid green line). The near-period-2 chaotic spiking activity can be interpreted as being produced by this structure. This frequency decreases as v_r further decreases ($v_r=0.12$ case indicated by the solid red line).

Fixing v_r at 0.33 in region #1 and v_r at 0.14 in region #2, we evaluate the dependence of $\psi(u_i)$ on the $u_{i+1} - u_i$ return map on parameter ε (Fig. 8). The stretching and folding structure with piecewise nearly linear maps appears, as shown in $\varepsilon=0.053$, in the case in which ε increases in region #1 (corresponding to the shape of the u -nullcline approaching the step function). A stretching and folding structure with non-linearity emerges at $u_i \approx 0.04$ when the ε values decrease, such as at $\varepsilon=0.05$, 0.03 . In region #2, nine folding structures appear at $\varepsilon=0.05$. The frequency of folding in this case decreases as the value of ε decreases (see $\varepsilon=0.045$, 0.04).

Discussion and Conclusion

In this paper, we applied the resetting process to a continuous 2D spiking neuron model with a sigmoidal nullcline structure to reveal the mechanisms for the emergence of chaotic states in a hybrid spiking neuron model. We also evaluated the bifurcation and routes to chaos against two types of spikes generated by the parameter sets for saddle-node bifurcation (region #1) and spikes for Hopf bifurcation (region #2) by changing the value of the resetting parameter. Through an evaluation using the Lyapunov exponent with a saltation matrix and the index for the fixed-point stability on a Poincaré section, we demonstrated that two types of chaotic behaviour are induced by the resetting process.

A chaotic state with bursting characteristics emerged in region #1 through tangent bifurcation, with a jump distance that increased as v_r decreased. This chaotic state moved to the periodic state through period-doubling bifurcation as the distance increased even further. We investigated the dependence of the return map on the

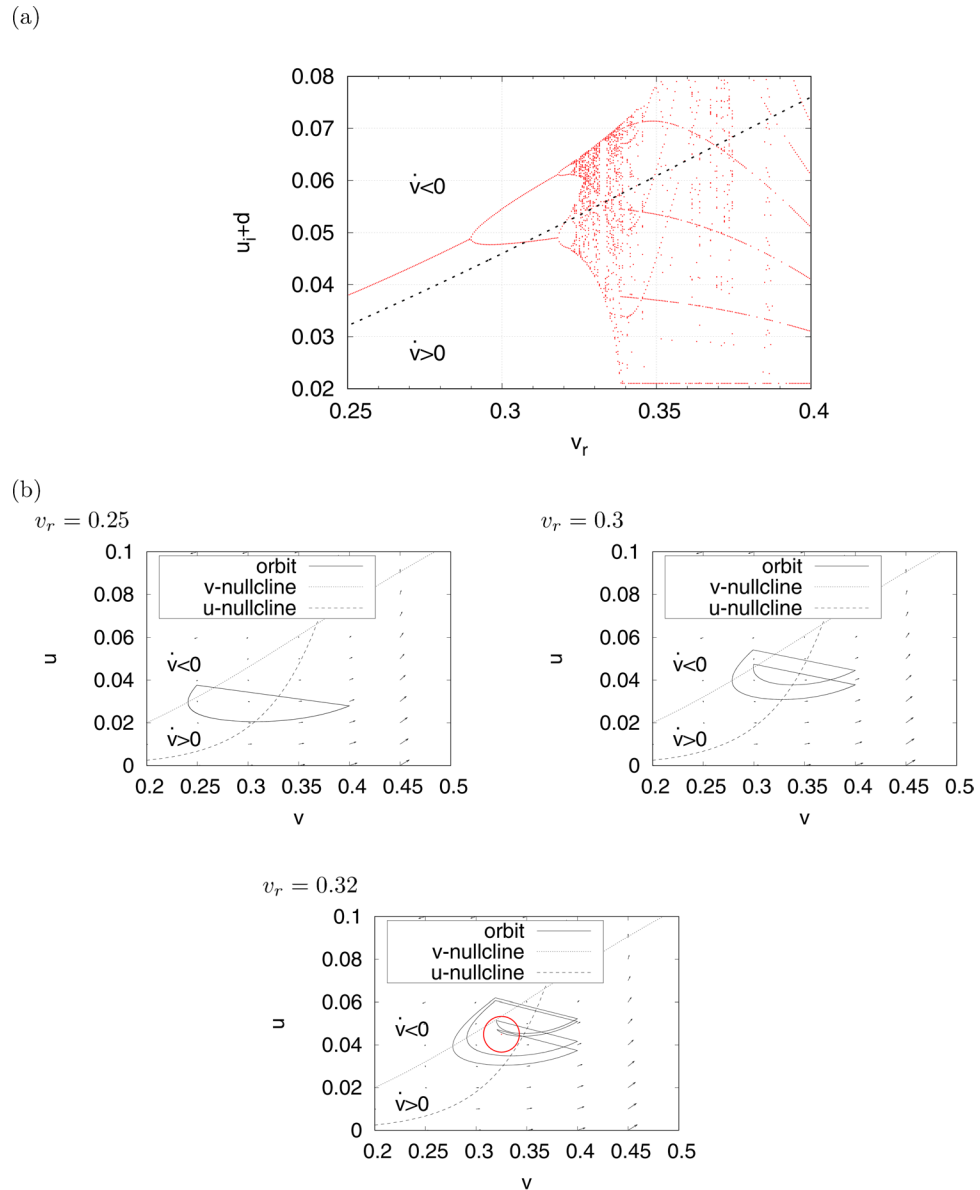


Figure 6. Transition scheme from spiking to bursting against changing v_r in region #1. (a) Bifurcation diagram of $u_i + d$ (the dotted line indicates v -nullcline) and (b) orbits (v, u) . The parameter values are similar to those in Figs 4 and 5 ($a = 0.1$, $\alpha = 0.1$, $\varepsilon = 0.05$, $\beta = 0.5$, $I = 0.004$, $v_{\text{peak}} = 0.4$, $d = 0.01$). The red circle in the graph for $v_r = 0.32$ indicates the region, where (v, u) jumps in $\dot{v} > 0$.

resetting parameter and compared the models with and without the resetting process. Consequently, we found that the non-linear stretching and folding structure of the attractor is induced by the resetting process. This structure is also affected by the shape of the sigmoidal function of the u -nullcline. We also confirmed that the bursting chaotic states emerged according to the adjustment of this structure's non-linearity.

Homoclinic orbits coexisting with fast and slow dynamics are needed to reproduce bursting³⁸. For example, using the Hindmarsh–Rose neuron model as a continuous three-dimensional spiking neuron model can reproduce the bursting by fast dynamics of the membrane potential and recovery variable and the slow dynamics of the bursting variable¹². Meanwhile, in hybrid spiking neuron models (Fig. 6) bursting can be reproduced using 2D systems because the hyperpolarization after resetting to $\dot{v} < 0$ and the depolarization in the inter-burst term after resetting to $\dot{v} > 0$ can play the roles of slow and fast dynamics, respectively. The analysis of the Hindmarsh–Rose neuron model indicated that a unimodal peak on the return map of the Poincaré section existed in chaotic bursting^{39–41}. This structure, which was also confirmed in region #1 of our model (Fig. 7(a)), contributes to the generation of chaotic bursting. Investigations of this chaotic bursting by inter-spike intervals (ISI) have previously been described in the literature^{42,43}. Gu⁴³ reported that the return map of the ISI exhibited a unimodal peak in chaotic bursting, with a peak value that decreased with the approach of chaotic spiking in a physiological experiment involving a neural pacemaker. Meanwhile, Innocenti *et al.*⁴² demonstrated that this return map has two peaks in

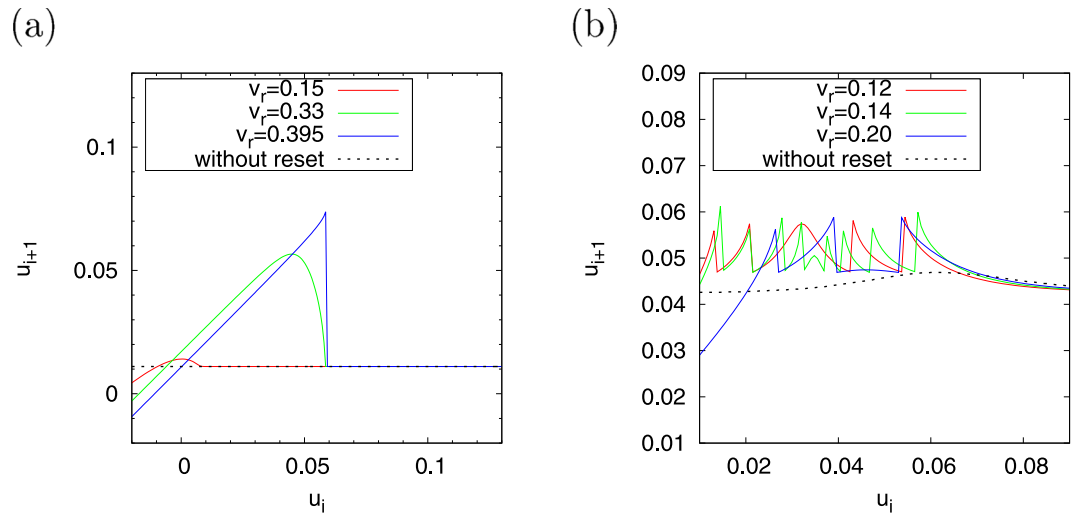


Figure 7. Dependence of the return map $u_{i+1} = \psi(u_i)$ on parameter v_r in regions #1 (a) and #2 (b). ($a = 0.1$, $\alpha = 0.1$, $\varepsilon = 0.05$, $d = 0.01$. Region #1: $\beta = 0.5$, $I = 0.004$ and $v_{\text{peak}} = 0.4$; and region #2: $\beta = 0.3$, $I = 0.04$ and $v_{\text{peak}} = 0.225$).

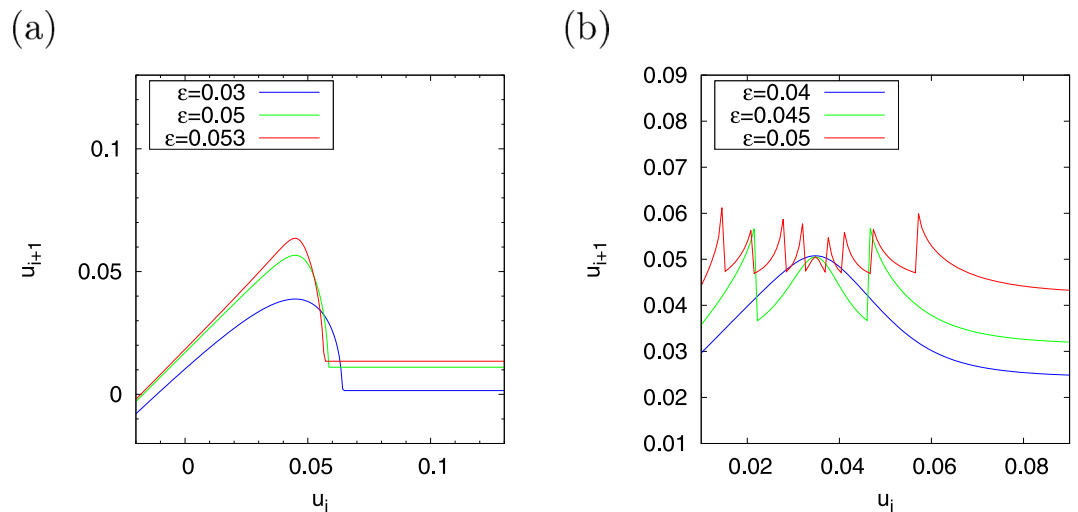


Figure 8. Dependence of the return map $u_{i+1} = \psi(u_i)$ on parameter ε in regions #1 (a) and #2 (b). ($a = 0.1$, $\alpha = 0.1$, $d = 0.01$. Region #1: $\beta = 0.5$, $I = 0.004$, $v_{\text{peak}} = 0.4$ and $v_r = 0.33$; and region #2: $\beta = 0.3$, $I = 0.04$, $v_{\text{peak}} = 0.225$ and $v_r = 0.14$).

chaotic bursting and that these peaks merged with the approach of chaotic spiking in the Hindmarsh–Rose neuron model. The patterns of the ISI prior to the last-minute hyperpolarization might be interpreted as reflecting the number of peaks in the return map. In our case, we confirmed that the trend in our result is consistent with that of Gu (Additional Information)⁴³.

A chaotic state with a near-period-2 behaviour emerged in region #2 through tangent bifurcation as the jump distance increased. As the distance was increased even further, this chaotic state moved to a periodic state through tangent bifurcation. Evaluation of the return map showed that this chaotic state emerged from the non-linear stretching and folding structure of the attractor induced by the resetting process. The folding frequency increased as the jump distance increased; also, this frequency decreased as the value of parameter ε decreased.

In conclusion, the resetting process provides and enhances non-linear effects in attractors, a result that cannot be achieved in continuous spiking neuron models of less than two dimensions. Chaotic states tend to arise when a state-dependent jump exists with an appropriate distance. The two types of chaotic behaviour and bifurcation mentioned above can also be observed in the widely used Izhikevich neuron model^{14,29,31}. Therefore, the effects induced by the resetting process revealed in this study might be utilised to generate various chaotic spiking patterns.

Further research based on this study should be undertaken to classify the types of transition from chaotic bursting to spiking and to evaluate the bifurcation and chaos in neural networks composed of hybrid spiking neurons.

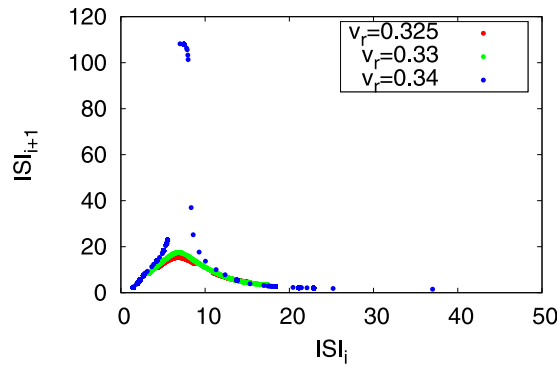


Figure 9. Return map of the inter-spike intervals (ISI) of chaotic bursting in region #1. ($a = 0.1$, $\alpha = 0.1$, $\varepsilon = 0.05$, $\beta = 0.5$, $I = 0.004$, $v_{\text{peak}} = 0.4$, $d = 0.01$).

Figure 9 shows the inter-spike intervals (ISI) $ISI_i = t_{i+1} - t_i$, where t_i indicates the spike time ($i = 0, 1, 2, \dots$) in the cases with the parameter settings for chaotic activity ($v_r = 0.325, 0.33, 0.34$) in region #1. As a result, the return map of the ISI exhibits a unimodal peak in chaotic bursting, and its peak value decreases with the approach of the parameter region of periodic bursting and spiking (Fig. 6).

References

- Rabinovich, M. I., Varona, P., Selverston, A. I. & Abarbanel, H. D. Dynamical principles in neuroscience. *Reviews of modern physics* **78**, 1213–1265 (2006).
- Hiratani, N., Teramae, J.-N. & Fukai, T. Associative memory model with long-tail-distributed hebbian synaptic connections. *Frontiers in computational neuroscience* **6** (2012).
- Mejias, J. & Longtin, A. Optimal heterogeneity for coding in spiking neural networks. *Physical Review Letters* **108**, 228102 (2012).
- Schweighofer, N., Lang, E. J. & Kawato, M. Role of the olivo-cerebellar complex in motor learning and control. *Front. Neural Circuits* **7**, 10–3389 (2013).
- Nobukawa, S. & Nishimura, H. Chaotic resonance in coupled inferior olive neurons with the Llinás approach neuron model. *Neural Computation* **28**, 2505–2532 (2016).
- Hodgkin, A. L. & Huxley, A. F. A quantitative description of membrane current and its application to conduction and excitation in nerve. *The Journal of physiology* **117**, 500–544 (1952).
- Magee, J. C. Dendritic hyperpolarization-activated currents modify the integrative properties of hippocampal ca1 pyramidal neurons. *Journal of Neuroscience* **18**, 7613–7624 (1998).
- Magistretti, J. & Alonso, A. Biophysical properties and slow voltage-dependent inactivation of a sustained sodium current in entorhinal cortex layer-II principal neurons. *The Journal of general physiology* **114**, 491–509 (1999).
- Dickson, C. T. *et al.* Properties and role of I_H in the pacing of subthreshold oscillations in entorhinal cortex layer II neurons. *Journal of Neurophysiology* **83**, 2562–2579 (2000).
- FitzHugh, R. Impulses and physiological states in theoretical models of nerve membrane. *Biophysical journal* **1**, 445–466 (1961).
- Nagumo, J., Arimoto, S. & Yoshizawa, S. An active pulse transmission line simulating nerve axon. *Proceedings of the IRE* **50**, 2061–2070 (1962).
- Hindmarsh, J. & Rose, R. A model of neuronal bursting using three coupled first order differential equations. *Proceedings of the Royal Society of London B: Biological Sciences* **221**, 87–102 (1984).
- Izhikevich, E. M. Simple model of spiking neurons. *IEEE Transactions on neural networks* **14**, 1569–1572 (2003).
- Izhikevich, E. M. Which model to use for cortical spiking neurons? *IEEE transactions on neural networks* **15**, 1063–1070 (2004).
- Aihara, K. & Suzuki, H. Theory of hybrid dynamical systems and its applications to biological and medical systems. *Philosophical Transactions of the Royal Society of London A: Mathematical, Physical and Engineering Sciences* **368**, 4893–4914 (2010).
- Coombes, S., & Thul, R. Wedgwood, K. Nonsmooth dynamics in spiking neuron models. *Physica D: Nonlinear Phenomena* **241**, 2042–2057 (2012).
- Badel, L. *et al.* Extracting non-linear integrate-and-fire models from experimental data using dynamic I–V curves. *Biological cybernetics* **99**, 361 (2008).
- Bernardo, M., Budd, C., Champneys, A. R. & Kowalczyk, P. *Piecewise-smooth dynamical systems: theory and applications*, vol. 163 (Springer Science & Business Media 2008).
- Mitsubori, K. & Saito, T. Dependent switched capacitor chaos generator and its synchronization. *IEEE Transactions on Circuits and Systems I: Fundamental Theory and Applications* **44**, 1122–1128 (1997).
- Nakano, H. & Saito, T. Basic dynamics from a pulse-coupled network of autonomous integrate-and-fire chaotic circuits. *IEEE Transactions on Neural Networks* **13**, 92–100 (2002).
- Yotsuji, K. & Saito, T. Basic analysis of a hyperchaotic spiking circuit with impulsive switching. *Nonlinear Theory and Its Applications, IEICE* **5**, 535–544 (2014).
- Kimura, K., Suzuki, S., Tsubone, T. & Saito, T. The cylinder manifold piecewise linear system: Analysis and implementation. *Nonlinear Theory and Its Applications, IEICE* **6**, 488–498 (2015).
- Tsubone, T., Saito, T. & Inaba, N. Design of an analog chaos-generating circuit using piecewise-constant dynamics. *Progress of Theoretical and Experimental Physics* **2016**, 053A01 (2016).
- Coombes, S. Liapunov exponents and mode-locked solutions for integrate-and-fire dynamical systems. *Physics Letters A* **255**, 49–57 (1999).
- Müller, P. C. Calculation of Lyapunov exponents for dynamic systems with discontinuities. *Chaos, Solitons & Fractals* **5**, 1671–1681 (1995).
- Pikovsky, A. & Politi, A. *Lyapunov exponents: a tool to explore complex dynamics* (Cambridge University Press 2016).
- Tamura, A., Ueta, T. & Tsuji, S. Bifurcation analysis of Izhikevich neuron model. *Dynamics of continuous, discrete and impulsive systems, Series A: mathematical analysis* **16**, 759–775 (2009).
- Bizzarri, F., Brambilla, A. & Gajani, G. S. Lyapunov exponents computation for hybrid neurons. *Journal of computational neuroscience* **35**, 201–212 (2013).

29. Nobukawa, S., Nishimura, H., Yamanishi, T. & Liu, J.-Q. Chaotic states induced by resetting process in Izhikevich neuron model. *Journal of Artificial Intelligence and Soft Computing Research* **5**, 109–119 (2015).
30. Nobukawa, S., Nishimura, H., Yamanishi, T. & Liu, J.-Q. Analysis of chaotic resonance in Izhikevich neuron model. *PLoS one* **10**, e0138919 (2015).
31. Nobukawa, S., Nishimura, H. & Yamanishi, T. Chaotic resonance in typical routes to chaos in the Izhikevich neuron model. *Scientific Reports* **7**, 1331 (2017).
32. Nobukawa, S., Nishimura, H. & Yamanishi, T. Chaotic states caused by discontinuous resetting process in spiking neuron model. In *Neural Networks (IJCNN), 2016 International Joint Conference on*, 315–319 (IEEE 2016).
33. Nobukawa, S., Nishimura, H. & Yamanishi, T. Analysis of chaos route in hybridized Fitzhugh–Nagumo neuron model. *Transactions of The Institute of Systems, Control and Information Engineers* (in Japanese) (2017).
34. Izhikevich, E. M. *Dynamical systems in neuroscience* (MIT press 2007).
35. Morris, C. & Lecar, H. Voltage oscillations in the barnacle giant muscle fiber. *Biophysical journal* **35**, 193–213 (1981).
36. Tsumoto, K., Kitajima, H., Yoshinaga, T., Aihara, K. & Kawakami, H. Bifurcations in Morris–Lecar neuron model. *Neurocomputing* **69**, 293–316 (2006).
37. Hindmarsh, A. C. *et al.* Sundials: Suite of nonlinear and differential/algebraic equation solvers. *ACM Transactions on Mathematical Software (TOMS)* **31**, 363–396 (2005).
38. Izhikevich, E. M. & Hoppensteadt, F. Classification of bursting mappings. *International Journal of Bifurcation and Chaos* **14**, 3847–3854 (2004).
39. Wang, X.-J. Genesis of bursting oscillations in the Hindmarsh–Rose model and homoclinicity to a chaotic saddle. *Physica D: Nonlinear Phenomena* **62**, 263–274 (1993).
40. González-Miranda, J. M. Observation of a continuous interior crisis in the Hindmarsh–Rose neuron model. *Chaos: An Interdisciplinary Journal of Nonlinear Science* **13**, 845–852 (2003).
41. Shilnikov, A. & Kolomiets, M. Methods of the qualitative theory for the Hindmarsh–Rose model: A case study—a tutorial. *International Journal of Bifurcation and chaos* **18**, 2141–2168 (2008).
42. Innocenti, G., Morelli, A., Genesio, R. & Torcini, A. Dynamical phases of the Hindmarsh–Rose neuronal model: Studies of the transition from bursting to spiking chaos. *Chaos: An Interdisciplinary Journal of Nonlinear Science* **17**, 043128 (2007).
43. Gu, H. Experimental observation of transition from chaotic bursting to chaotic spiking in a neural pacemaker. *Chaos: An Interdisciplinary Journal of Nonlinear Science* **23**, 023126 (2013).

Acknowledgements

This work was supported by the JSPS KAKENHI Grant-in-Aid for Young Scientists (B) grant number 15K21471.

Author Contributions

S.N., T.Y. and H.N. devised the methods; S.N. conducted the experiments; and S.N. and H.N. analysed the results. All authors reviewed the manuscript.

Additional Information

Competing Interests: The authors declare that they have no competing interests.

Publisher's note: Springer Nature remains neutral with regard to jurisdictional claims in published maps and institutional affiliations.



Open Access This article is licensed under a Creative Commons Attribution 4.0 International License, which permits use, sharing, adaptation, distribution and reproduction in any medium or format, as long as you give appropriate credit to the original author(s) and the source, provide a link to the Creative Commons license, and indicate if changes were made. The images or other third party material in this article are included in the article's Creative Commons license, unless indicated otherwise in a credit line to the material. If material is not included in the article's Creative Commons license and your intended use is not permitted by statutory regulation or exceeds the permitted use, you will need to obtain permission directly from the copyright holder. To view a copy of this license, visit <http://creativecommons.org/licenses/by/4.0/>.

© The Author(s) 2017